THE JOURNAL OF BIOLOGICAL CHEMISTRY VOL. 290, NO. 34, pp. 21054–21066, August 21, 2015

Dimerization Mediated by a Divergent Forkhead-associated Domain Is Essential for the DNA Damage and Spindle Functions of Fission Yeast Mdb1*

Received for publication, January 31, 2015, and in revised form, July 5, 2015 Published, JBC Papers in Press, July 9, 2015, DOI 10.1074/jbc.M115.642538

Shukun Luo (罗树坤)[‡1], Xiaoran Xin (信潇然)[‡1], Li-Lin Du (杜立林)[‡2], Keqiong Ye (叶克穷)[‡§3], and Yi Wei (魏祎)[‡1]

From the [‡]National Institute of Biological Sciences, Beijing 102206, China and the [§]Key Laboratory of RNA Biology, Institute of Biophysics, Chinese Academy of Sciences, Beijing 100101, China

Background: Fission yeast Mdb1 is homologous to mammalian MDC1, but the extent of conservation is unclear.
Results: A previously unrecognized FHA domain in Mdb1 mediates a functionally important homodimerization.
Conclusion: FHA domain-mediated dimerization is a conserved feature of MDC1 family proteins.
Significance: This study extends our understanding of the function, mechanism, and evolution of MDC1 family proteins.

MDC1 is a key factor of DNA damage response in mammalian cells. It possesses two phospho-binding domains. In its C terminus, a tandem BRCA1 C-terminal domain binds phosphorylated histone H2AX, and in its N terminus, a forkhead-associated (FHA) domain mediates a phosphorylation-enhanced homodimerization. The FHA domain of the *Drosophila* homolog of MDC1, MU2, also forms a homodimer but utilizes a different dimer interface. The functional importance of the dimerization of MDC1 family proteins is uncertain. In the fission yeast *Schizosaccharomyces pombe*, a protein sharing homology with MDC1 in the tandem BRCA1 C-terminal domain, Mdb1, regulates DNA damage response and mitotic spindle functions. Here, we report the crystal structure of the N-terminal 91 amino acids of Mdb1. Despite a lack of obvious sequence conservation to the FHA domain of MDC1, this region of Mdb1 adopts an FHA-like fold and is therefore termed Mdb1-FHA. Unlike canonical FHA domains, Mdb1-FHA lacks all the conserved phospho-binding residues. It forms a stable homodimer through an interface distinct from those of MDC1 and MU2. Mdb1-FHA is important for the localization of Mdb1 to DNA damage sites and the spindle midzone, contributes to the roles of Mdb1 in cellular responses to genotoxins and an antimicrotubule drug, and promotes *in vitro* binding of Mdb1 to a phospho-H2A peptide. The defects caused by the loss of Mdb1-FHA can be rescued by fusion with either of two heterologous dimerization domains, suggesting that the main function of Mdb1-FHA is mediating dimerization. Our data support that FHA-mediated dimerization is conserved for MDC1 family proteins.

Eukaryotic DNA damage response relies heavily on protein phosphorylation events, which are often recognized by phospho-binding domains (1, 2). One of the earliest DNA break-induced events is the phosphorylation of histone H2AX (histone H2A in yeasts) (3). Phospho-H2AX, known as γH2AX, serves as a recruiting platform for checkpoint signaling proteins and DNA repair proteins (4). In mammalian cells, the recruiting role of γH2AX is mainly mediated by MDC1, which directly binds to γH2AX through its C-terminal tBRCT domain (5–7).

In addition to the tBRCT domain, MDC1 contains a second phospho-binding domain, an FHA[4] domain, in its N terminus. Recently, four studies, including three that solved the crystal structures of the MDC1-FHA domain, demonstrated that MDC1 can self-associate through the FHA domain (8–11). The structures revealed that MDC1-FHA has an intrinsic ability to form a homodimer. Furthermore, an intersubunit interaction between MDC1-FHA and a phosphorylation site near the extreme N terminus of MDC1 enhances the dimerization (10, 11). The exact physiological function of the dimerization of MDC1 remains unresolved, because two studies showed that loss of dimerization partially impairs the ability of MDC1 to localize to DNA damage sites (8, 10), whereas another study concluded that dimerization does not contribute to MDC1 accumulation at sites of DNA breaks (11).

The FHA domain in the *Drosophila* ortholog of MDC1, MU2, was found to also forms a homodimer (12), raising the possibility that dimerization is an ancient and conserved function of the FHA domains in MDC1 family proteins. However, the dimerization interface of MU2-FHA is completely different from that of MDC1-FHA, and because of a lack of phospho-binding residues, the dimerization of MU2-FHA is probably

* This work was supported by Chinese Ministry of Science and Technology 863 Project 2008AA022310 and 973 Project 2010CB835402 (to K. Y.) and 863 Project 2007AA02Z1A5 (to L.-L. D.), by National Natural Science Foundation of China Grant 31325007 (to K. Y.), and by the Beijing Municipal Government. The authors declare that they have no conflicts of interest with the contents of this article.
The atomic coordinates and structure factors (code 4S3H) have been deposited in the Protein Data Bank (http://wwpdb.org/).
[1] These authors contributed equally to this work.
[2] To whom correspondence may be addressed: National Inst. of Biological Sciences, 7 Science Park Rd., Zhongguancun Life Science Park, Beijing 102206, China. Tel.: 86-10-80726688, Ext. 8505; Fax: 86-10-80720499; E-mail: dulilin@nibs.ac.cn.
[3] To whom correspondence may be addressed: National Inst. of Biological Sciences, 7 Science Park Rd., Zhongguancun Life Science Park, Beijing 102206, China. Tel.: 86-10-80726688, Ext. 8550; Fax: 86-10-80728592; E-mail: yekeqiong@nibs.ac.cn.

[4] The abbreviations used are: FHA, forkhead-associated; rmsd, root mean square deviation; tBRCT, tandem BRCA1 C-terminal; IR, ionizing radiation; CPT, camptothecin; LZ, leucine zipper motif; GBP, GFP-binding protein; TBZ, thiabendazole.

not subject to phospho-regulation like that of MDC1-FHA. Therefore, it seems equally plausible that MDC1-FHA and MU2-FHA have independently acquired the ability to dimerize during evolution. The physiological importance of MU2 dimerization has not been addressed.

In the fission yeast *Schizosaccharomyces pombe*, phospho-H2A (γH2A) is directly recognized by three tBRCT domain-containing proteins: Crb2 (13–16), Brc1 (17, 18), and Mdb1 (19). Among them, Mdb1 shares with MDC1 the highest level of sequence similarity, which is limited to the tBRCT domain (19). Mdb1 not only modulates DNA damage response in a γH2A-dependent manner but also influences mitotic spindle function in a γH2A-independent manner (19). The N-terminal region of Mdb1 shows conservation among fission yeast species, but no sequence homology can be detected beyond the *Schizosaccharomyces* genus, nor can any known domain be identified in this region using various domain-searching tools.

Here, we report the crystal structure of the N-terminal 91 amino acids of Mdb1. We show that this region of Mdb1 folds into a FHA domain and forms a stable homodimer. The dimerization function of this domain is important for the roles of Mdb1 in DNA damage response and mitotic spindle regulation. Our findings suggest that FHA-mediated dimerization is a universal and conserved property of MDC1 family proteins.

Experimental Procedures

Gene Cloning and Protein Purification—The DNA sequence encoding Mdb1 (a total of 624 residues) was PCR amplified from a *S. pombe* cDNA library and cloned into a pET-15b plasmid with an N-terminal His_6 tag and a thrombin cleavage site. Two FHA domain fragments with residues 1–104 and 1–91 were cloned into a modified pET-28a vector and fused to an N-terminal His_6 tag followed by a PreScission cleavage site.

All proteins were expressed in *Escherichia coli* BL21(DE3) strain (Novagen) induced with 0.2 mM isopropyl β-D-thiogalactopyranoside. The full-length protein was expressed at 37 °C for 4 h, whereas two FHA fragments were expressed at 25 °C for 12 h. To purify Mdb1(1–104), harvested cells were resuspended in buffer P300 (50 mM sodium phosphate, pH 7.6, 300 mM KCl) and lysed by sonication. After centrifugal clarification, the supernatant was loaded onto a 5-ml HisTrap column (GE Healthcare), which was then washed with 20 mM imidazole in P300. The proteins were eluted with 500 mM imidazole in P300. After 6-fold dilution with 25 mM HEPES-KOH, pH 7.6, proteins were loaded onto a HiTrap Q column and eluted with a 0–1 M KCl gradient in 25 mM HEPES-KOH, pH 7.6. The target protein was collected, concentrated with Amicon Ultra-15 centrifugal filter units (3-kDa cutoff; Millipore), and further purified with a Superdex 75 column run in 5 mM HEPES-KOH, pH 7.6, 100 mM KCl.

Full-length Mdb1 and Mdb1(1–91) were expressed and purified in the same way but did not undergo the final step of gel filtration chromatography. The His_6 tag of Mdb1(1–91) was cleaved with PreScission protease at 4 °C for 4 h after HisTrap chromatography, and uncleaved protein was removed by a HisTrap column. Protein concentrations were calculated based on absorbance at 280 nm measured using a NanoDrop photospectrometer and theoretical molar extinction coefficients predicted by ExPaSy.

Crystallization and Structure Determination—Mdb1(1–104) with an uncleaved His_6 tag was crystallized at 20 °C using the hanging drop vapor diffusion approach. One μl of protein sample (35 mg/ml in 5 mM HEPES-KOH, pH 7.6, 100 mM KCl) was mixed with 1 μl of reservoir solution containing 0.1 M sodium acetate, pH 5.2, and 1.8 M ammonium sulfate. Diamond-shaped crystals appeared in 2 days and were harvested after 1 week. Mercury derivatives were prepared by soaking crystals in the reservoir solution containing 1 mM merthiolate sodium for 6 h. Crystals were cryoprotected in the reservoir solution supplemented with 25% glycerol and flash cooled in liquid nitrogen.

Data were collected at 100 K at Beamline 3W1A of the Beijing Synchrotron Radiation Facility and processed with HKL2000 (20). The structure was determined by the single-wavelength anomalous diffraction method using a mercury derivative data set collected at a wavelength of 1.009 Å. Heavy atom search, phase calculation, and density modification were conducted in autoSHARP (21). Model building and refinement were conducted using Coot, Refmac, and Phenix (22–24). The model was refined against a native data set to 2.7 Å resolution. The current model contains 4 Mdb1-FHA molecules with residues 1–22 and 26–91, residues 1–12 and 15–91, residues 1–90, and residues 1–90, as well as 3 sulfate ions and 20 water molecules. RAMPAGE analysis shows that 95.1% of the residues are in favored region and 4.9% in allowed region. Structural figures were created with PyMOL (25).

Limited Proteolysis and Mass Spectrometry—Approximately 10 mg of full-length Mdb1 protein was incubated with 160 μg of trypsin in 10 ml of P300 buffer at 4 °C. After 12 h of digestion, the reaction was concentrated and loaded onto a Superdex 75 Hiload 16/60 column equilibrated in 50 mM sodium phosphate, pH 7.6, 150 mM NaCl at 4 °C. Peak fractions were analyzed with SDS-PAGE. The main cleavage products were identified with mass spectrometry. Size exclusion columns were calibrated with protein standards: bovine serum albumin (67 kDa), ovalbumin (43 kDa), chymotrypsinogen (25 kDa), and lysozyme (14.4 kDa).

Sedimentation Equilibrium—The sedimentation equilibrium experiments were performed with an XL-I analytical ultracentrifuge (Beckman Coulter) equipped with an An-60 Ti rotor and a six-channel centerpiece. Mdb1(1–91) with no tag was exchanged to 20 mM sodium phosphate, pH 7.6, and 150 mM NaCl with gel filtration and loaded at a monomer concentration of 67 μM to middle cells and at a monomer concentration of 34 μM to outer cells. The samples were centrifuged at 25 °C with 25,000, 30,000, and 38,000 rpm and detected using absorbance at 280 nm. All data were globally fit using a self-association model in SedPhat program as described previously (10).

Accession Number—The atomic coordinates and structure factors of Mdb1 FHA structure have been deposited in the Protein Data Bank under accession code 4S3H.

Fission Yeast Strains—Fission yeast strains used in this study are listed in Table 1. Methods for strain construction and composition of media are as described (26). For the construction of plasmids expressing wild-type or truncated Mdb1, the Mdb1 coding sequence was amplified by PCR and inserted into mod-

TABLE 1
Fission yeast strains used in this study

Strain	Mating type	Genotype
LD327	*h*−	*his3-D1*
DY15603	*h*+	*his3-D1 mdb1Δ::hphMX leu1-32::P81nmt1-Mdb1-wt-GFP (leu1+)*
DY15615	*h*+	*ura4-D18 his3-D1 leu1-32::Pnmt1-GFP (leu1+)*
DY15616	*h*+	*ura4-D18 his3-D1 leu1-32::Pnmt1-Mdb1-wt-GFP (leu1+)*
DY15627	*h*+	*his3-D1 mdb1Δ::hphMX ars1::CFP-atb2::LEU2 leu1-32::P81nmt1-Mdb1-wt-GFP (leu1+)*
DY15630	*h*+	*his3-D1 mdb1Δ::hphMX leu1-32::P81nmt1-GFP (leu1+)*
DY15638	*h*+	*his3-D1 mdb1Δ::hphMX leu1-32::P81nmt1-Mdb1 (105–624)-GFP (leu1+)*
DY16307	*h*+	*his3-D1 mdb1Δ::hphMX leu1-32::P81nmt1-LZ-Mdb1 (105–624)-GFP (leu1+)*
DY16309	*h*+	*his3-D1 mdb1Δ::hphMX leu1-32::P81nmt1-GST-Mdb1 (105–624)-GFP (leu1+)*
DY16573	*h*−	*ura4-D18 his3-D1 (?) crb2 (1–778)F400A mdb1Δ::natMX leu1-32::P81nmt1-GST-Mdb1 (105–624)-GFP (leu1+)*
DY16579	*h*−	*ura4-D18 his3-D1 (?) crb2 (1–778)F400A mdb1Δ::natMX leu1-32::P81nmt1-LZ-Mdb1 (105–624)-GFP (leu1+)*
DY16581	*h*−	*ura4-D18 his3-D1 (?) crb2 (1–778)F400A mdb1Δ::natMX leu1-32::P81nmt1-GFP (leu1+)*
DY16639	*h*+	*his3-D1 mdb1Δ::hphMX ars1::CFP-atb2::LEU2 leu1-32::P81nmt1-Mdb1 (105–624)-GFP (leu1+)*
DY16643	*h*+	*his3-D1 mdb1Δ::hphMX ars1::CFP-atb2::LEU2 leu1-32::P81nmt1-GST-Mdb1 (105–624)-GFP (leu1+)*
DY16645	*h*+	*his3-D1 mdb1Δ::hphMX ars1::CFP-atb2::LEU2 leu1-32::P81nmt1-LZ-Mdb1 (105–624)-GFP (leu1+)*
DY17124	*h*−	*ura4-D18 his3-D1 (?) crb2 (1–778)F400A mdb1Δ::natMX leu1-32::P81nmt1-Mdb1-wt-GFP (leu1+)*
DY17126	*h*−	*ura4-D18 his3-D1 (?) crb2 (1–778)F400A mdb1Δ::natMX leu1-32::P81nmt1-Mdb1 (105–624)-GFP (leu1+)*
DY17216	*h*+	*ura4-D18 his3-D1 leu1-32::Pnmt1-Mdb1 (105–624)-GFP (leu1+)*
DY17218	*h*+	*ura4-D18 his3-D1 leu1-32::Pnmt1-GST-Mdb1 (105–624)-GFP (leu1+)*
DY17220	*h*+	*ura4-D18 his3-D1 leu1-32::Pnmt1-LZ-Mdb1 (105–624)-GFP (leu1+)*
DY18067	*h*+	*his3-D1 mdb1Δ::hphMX leu1-32::P81nmt1-GFP-Mdb1-wt (leu1+) ars1::P81nmt1-mCherry-Mdb1-wt (his3+)*
DY18069	*h*+	*his3-D1 mdb1Δ::hphMX leu1-32::P81nmt1-GFP-Mdb1-wt (leu1+) ars1::P81nmt1-mCherry-Mdb1 (105–624) (his3+)*
DY23263	*h*+	*ura4-D18 leu1-32 mdb1Δ::hphMX leu1-32::P81nmt1-Mdb1(105–624)-wt-GFP(leu1+) his3::Ptub1-Mdb1(105–624)-wt-GBP(kanMX)*
DY24110	*h*+	*ura4-D18 leu1-32 mdb1Δ::hphMX leu1-32::P81nmt1-Mdb1(105–624)-wt-GFP(leu1+) his3::Ptub1-Mdb1(105–624)-K434* M-GBP(kanMX)
DY24112	*h*+	*ura4-D18 leu1-32 mdb1Δ::hphMX leu1-32::P81nmt1-Mdb1(105–624)-K434* M-GFP(leu1+) his3::*Ptub1-Mdb1(105–624)-wt-GBP(kanMX)*
DY24114	*h*+	*ura4-D18 leu1-32 mdb1Δ::hphMX leu1-32::P81nmt1-Mdb1(105–624)-K434* M-GFP(leu1+) his3::*Ptub1-Mdb1(105–624)-K434* M-GBP(kanMX)
DY24566	*h*+	*leu1-32 his3-D1 mdb1Δ::hphMX leu1-32::P81nmt1-GFP-GST-Mdb1 (105–624) (leu1+) ars1::P81nmt1-mCherry-Mdb1 (105–624) (his3+)*
DY24567	*h*+	*leu1-32 his3-D1 mdb1Δ::hphMX leu1-32::P81nmt1-GFP-GST-Mdb1 (105–624) (leu1+) ars1::P81nmt1-mCherry-GST-Mdb1 (105–624) (his3+)*
DY24570	*h*+	*leu1-32 his3-D1 mdb1Δ::hphMX leu1-32::P81nmt1-GFP-LZ-Mdb1 (105–624) (leu1+) ars1::P81nmt1-mCherry-Mdb1 (105–624) (his3+)*
DY24571	*h*+	*leu1-32 his3-D1 mdb1Δ::hphMX leu1-32::P81nmt1-GFP-LZ-Mdb1 (105–624) (leu1+) ars1::P81nmt1-mCherry-LZ-Mdb1 (105–624) (his3+)*

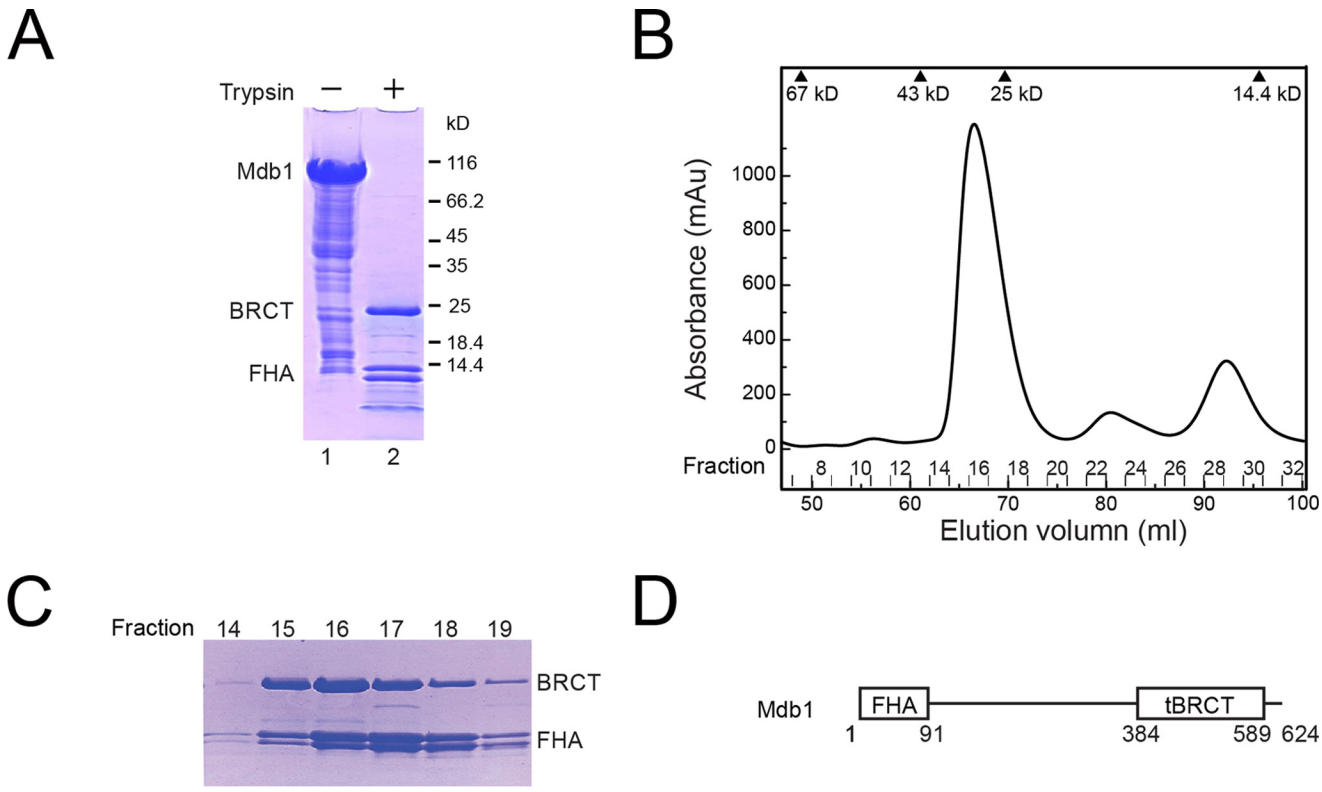

FIGURE 1. **Domain organization of Mdb1.** *A*, full-length Mdb1 protein was partially digested with trypsin and analyzed with SDS-PAGE and Coomassie staining. The migration positions of molecular makers are indicated. *B*, elution profile of Mdb1 digestion products in a Superdex 75 column. The elution positions of protein standards are indicated. *C*, peak fractions from gel filtration of trypsin-digested Mdb1 were analyzed with SDS-PAGE. *D*, domain diagram of Mdb1.

ified pDUAL vectors (19, 27), which contain one of the three versions of thiamine-repressible *nmt1* promoter (*Pnmt1*, *P41nmt1*, or *P81nmt1*) and the sequence encoding GFP or mCherry. Sequences of heterologous dimerization domains were identical to the ones previously used for Crb2 fusions (28). The plasmids were linearized with NotI and integrated at the *leu1* locus or were linearized with MluI and integrated at the *ars1* locus. For the strains containing CFP-tubulin (CFP-Atb2), pREP81-CFP-atb2 was linearized with MluI and integrated at the *ars1* locus (19).

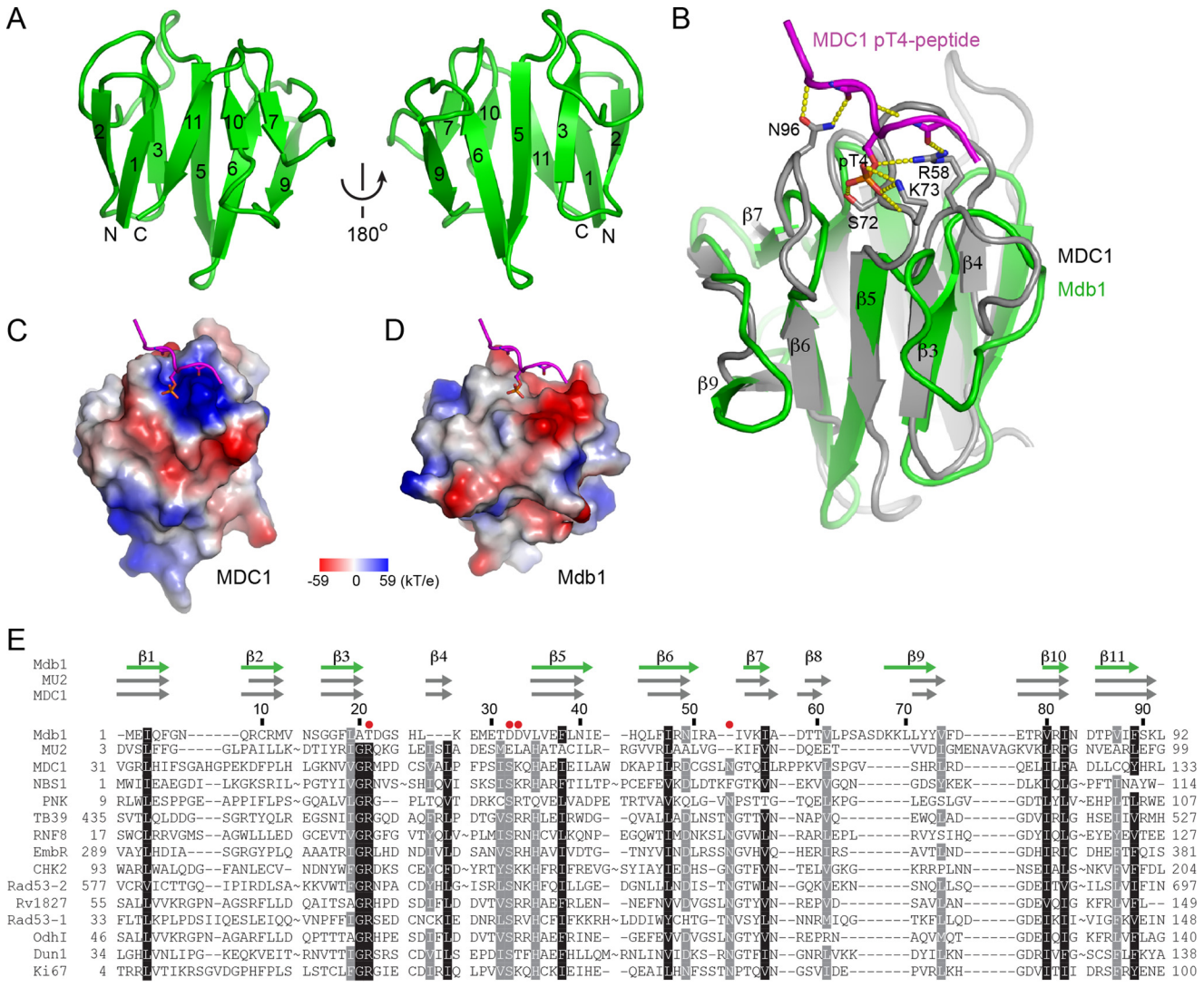

FIGURE 2. **Structure of the FHA domain of Mdb1.** *A*, ribbon representation of the FHA domain of Mdb1. Two opposite views are displayed. The β-strands are numbered according to structural equivalence to those of canonical FHA domains. The N and C termini are labeled. *B*, Mdb1-FHA lacks a Thr(P)-binding pocket. The structure of Mdb1-FHA is superimposed with the structure of MDC1-FHA bound with the MDC1-Thr(P)-4 peptide (Protein Data Bank code 3UNN). The interacting residues in the MDC1 FHA-phosphopeptide complex are shown in a stick and ball representation with phosphorus colored *yellow*, oxygen *red*, and nitrogen *blue*. Hydrogen bonds are shown as *dashed lines*. *C* and *D*, charge surfaces of the FHA domains of MDC1 (*C*) and Mdb1 (*D*). The surfaces are colored from *blue* to *red* for positively to negatively charged regions. The two structures have the same orientation as in *B*. The phosphopeptide ligand of MDC1 is displayed in the Mdb1 structure to indicate the region corresponding to the Thr(P)-binding pocket in MDC1. *E*, structure-based sequence alignment of FHA domains. Aligned are FHA domains from the following (Protein Data Bank codes are shown in parentheses): Mdb1 (4S3H), MU2 (3UV0), MDC1 (3UNN), NBS1 (3HUF), PNK (2W3O), TB39.8 (3POA), RNF8 (2PIE), EmbR (2FF4), CHK2 (1GXC), Rad53-FHA1 (1G6G), Rv1827 (2KFU), Rad53-FHA2 (1J4L), OdhI (2KB3), Dun1 (2JQL), and Ki67 (2AFF). Except for Mdb1 and MU2, all FHA domains bind a phosphopeptide in structure. The key phosphopeptide-binding residues are marked with *red solid cycles*. The secondary structures are indicated for FHA domains of Mdb1 (*green arrows*), MU2 (*gray arrows*), and MDC1 (*gray arrows*) above the sequences. Residue numbers are shown for Mdb1. Omitted residues are indicated by ~. Residues that are conserved in at least 90 and 80% of these sequences are *shaded* in *black* and *gray*, respectively.

DNA Damage and Thiabendazole Sensitivity Assay—Cultures were grown to log phase and serial 5-fold dilutions of cells were spotted onto control and drug-containing plates. UV irradiation was applied using a CL-1000 UV crossy-linker (UVP). For ionizing radiation (IR) treatment, cells were irradiated with a Gammacell 1000 irradiator (dose rate, 16 Gy/min) in microcentrifuge tubes and then plated on YES plates.

Light Microscopy—Live cells were imaged using a 100×, 1.4-NA objective on a DeltaVision PersonalDV system (Applied Precision) equipped with a CFP/YFP/mCherry filter set (Chroma 89006 set) and a Photometrics CoolSNAP HQ2 camera. Images were analyzed with the SoftWoRx software.

Immunoprecipitation—Approximately 100 A_{600} units of log phase cells were grown in thiamine-free EMM medium. Cell lysates were prepared with the FastPrep system (MP Biomedicals) in the lysis buffer (50 mM HEPES, pH 7.5, 1 mM EDTA, 150 mM NaCl, 10% glycerol, 1 mM PMSF, 1 mM DTT, 0.05% Nonidet P-40, 1× Roche protease inhibitor mixture). RFP-trap-agarose beads (ChromoTek) were used for immunoprecipitating the mCherry-tagged protein. After washing the beads three times with lysis buffer, proteins bound to beads were eluted by boiling in SDS-PAGE loading buffer.

In Vitro γH2A Binding Assay—His_6-tagged Mdb1 proteins were expressed in *E. coli* strain BL21 and purified using nickel-

TABLE 2
Data collection and refinement statistics
The values for the data in the highest resolution bin are shown in parentheses.

	Hg derivative	Native
Data collection		
Space group	$P6_522$	$P6_522$
Cell dimensions		
a, *b*, *c* (Å)	90.7, 90.7, 224.0	91.1, 91.1, 224.5
α, β, γ (°)	90, 90, 120	90, 90, 120
Wavelength (Å)	1.009	1.000
Resolution range (Å)	25–2.70 (2.8–2.70)	20–2.70 (2.80–2.70)
Unique reflections	15,784 (1,496)	15,871 (1,524)
Redundancy	10.0 (7.2)	9.6 (9.9)
$<I>/<\sigma(I)>$	27.6 (3.35)	22.8 (3.4)
Completeness (%)	99.6 (96.9)	99.9 (99.8)
R_{merge}	0.073 (0.372)	0.102 (0.673)
Structure refinement		
Resolution range (Å)		20–2.70 (2.87–2.70)
No. reflections		15,820 (1,558)
No. atoms		2,918
R_{work}		0.219 (0.256)
R_{free}		0.271 (0.310)
rmsd bond length (Å)		0.011
rmsd bond angles (°)		1.623

nitrilotriacetic acid beads (Qiagen) in accordance with manufacturer's instructions. H2A peptide pull down assay was performed as previously described (19).

Results

Mdb1 Contains Two Structural Cores—To probe the structural cores of Mdb1, its full-length protein was partially digested with trypsin. We found three major products that were highly resistant to digestion and probably formed stable structural cores (Fig. 1*A*). Peptide sequencing by mass spectrometry showed that the product that migrated as a 25-kDa species in SDS-PAGE gel corresponded to the C-terminal tBRCT domain with residues 384–589 and two smaller products of ~14 kDa contained N-terminal residues 1–104 and 1–91. Gel filtration chromatography of digestion products showed that the N- and C-terminal products eluted with slightly different peaks at fractions 17 and 16, respectively (Fig. 1, *B* and *C*), suggesting that they were structurally independent after the linker region was removed. The tBRCT domain migrated in gel filtration column as expected for a monomer. By contrast, the N-terminal products eluted with an apparent molecular mass of ~30 kDa, which is more than twice its theoretical molecular mass of 12 kDa, suggesting that it may form a dimer in solution. Therefore, Mdb1 contains two structural cores at two extremes of the polypeptide (Fig. 1*D*).

The N-terminal Region of Mdb1 Is an Atypical FHA Domain—To gain insight into the structure and function of the N-terminal region of Mdb1, we expressed, purified, and crystallized a fragment containing residues 1–104 and determined its structure using a mercury derivative and the single-wavelength anomalous diffraction phasing method. The structure was refined to 2.7 Å resolution with an R_{work}/R_{free} of 0.219/0.271 and good geometric parameters (Fig. 2 and Table 2).

The asymmetric unit contains four molecules that each spans residues 1–91. Several residues in loop regions were not modeled in two protomers because of a lack of electron density. The four structures can be aligned with each other with root mean square deviations (rmsd) of ~0.4 Å over all Cα pairs. Search in the DaliLite server revealed that the structure is homologous to many FHA domains, with the MDC1 FHA domain being the top hit (Z score = 8.4, rmsd = 1.134 Å over 27 Cα pairs) (29). This homology cannot be identified at the sequence level. Our finding indicates that the similarity between Mdb1 and MDC1 extends to their N-terminal regions. We hereafter refer to the N-terminal domain of Mdb1 as Mdb1-FHA.

The canonical FHA domain contains 11 β-strands that assemble into two β-sheets and form a β-sandwich. In Mdb1-FHA, the equivalents of strands β4 and β8 are missing (Fig. 2*A*). For ease of comparison with other FHA structures, we label the β-strands in Mdb1-FHA according to their structural equivalence to the strands in the canonical 11-stranded fold. Thus, one β-sheet in Mdb1-FHA is composed of strands β3, β5, β6, and β9, and the other β-sheet is composed of strands β2, β1, β11, β10, and β7.

The phosphopeptide binding pocket of MDC1-FHA is composed of β3-β4, β4-β5, and β6-β7 loops (9–11). Residues Arg-58, Ser-72, Lys-73, and Asn-96 of MDC1 mediate critical interactions with a MDC1 peptide containing phosphorylated Thr-4 (Fig. 2*B*) and are highly conserved in FHA domains (Fig. 2*E*). However, in Mdb1-FHA, the β4 strand is missing, and the loop between β3 and β5 folds back to the body of β-sandwich, rather than occupying the equivalent position of β3-β4 and β4-β5 loops in canonical FHA domains (Fig. 2*B*). Three Thr(P)-binding residues, Arg-58, Ser-72, and Lys-73, in MDC1-FHA are replaced by Thr-21, Asp-32, and Asp-33 in Mdb1-FHA, respectively (Fig. 2*E*). Moreover, Mdb1, like MU2, has a shortened β6-β7 loop and lacks the equivalent of MDC1 Asn-96 (Fig. 2*E*). The Thr(P) binding pocket of MDC1-FHA is positively charged, whereas the corresponding region in Mdb1-FHA is partly negatively charged and partly neutral (Fig. 2, *C* and *D*). These structural features strongly suggest that Mdb1-FHA is incapable of binding phosphopeptides.

Mdb1-FHA Forms a Homodimer through a Novel Interface—Consistent with the results of gel filtration analysis (Fig. 1 and data not shown), the four Mdb1-FHA molecules in the asymmetric unit form two homodimers. The two dimers have identical dimer interface and can be aligned as a whole unit with an rmsd of 0.343 Å over all Cα pairs. In the dimer, two FHA subunits (named A and B) associate through parallel pairing of β9 strands (Fig. 3*A*). There are five hydrogen bonds connecting the polypeptide backbones of two β9 strands (Fig. 3*B*). In addition, at both sides of the β9 pair, residues from strands β5, β6, and β9 of one subunit contact with residues from strand β9 and its connecting loops to β7 and β10 of the other subunit. Specifically, residues Leu-39, Ile-41, Phe-46, Leu-71, and Tyr-73 of subunit A form a hydrophobic core with residues Leu-62′, Leu-70′, Tyr-72′, and Phe-75′ of subunit B (residues from subunit B are denoted by prime) at one side (Fig. 3*B*). At the other side of the β9 pair, the same set of residues from respective subunits also constitute a hydrophobic core. However, the alignment of equivalent residues at the interface is shifted by ~6 Å at two sides of the β9 pair (Fig. 3*B*). In addition, Gln-44 makes hydrogen bonds with Tyr-72′ and the carbonyl group of Thr-60′ at one side (Fig. 3*B*, *top*), whereas Gln-44′ hydrogen bonds with the side chain hydroxyl of Thr-59 at the other side (Fig. 3*B*, *bottom*). The dimerization interaction is asymmetric at two sides because the two subunits are not related

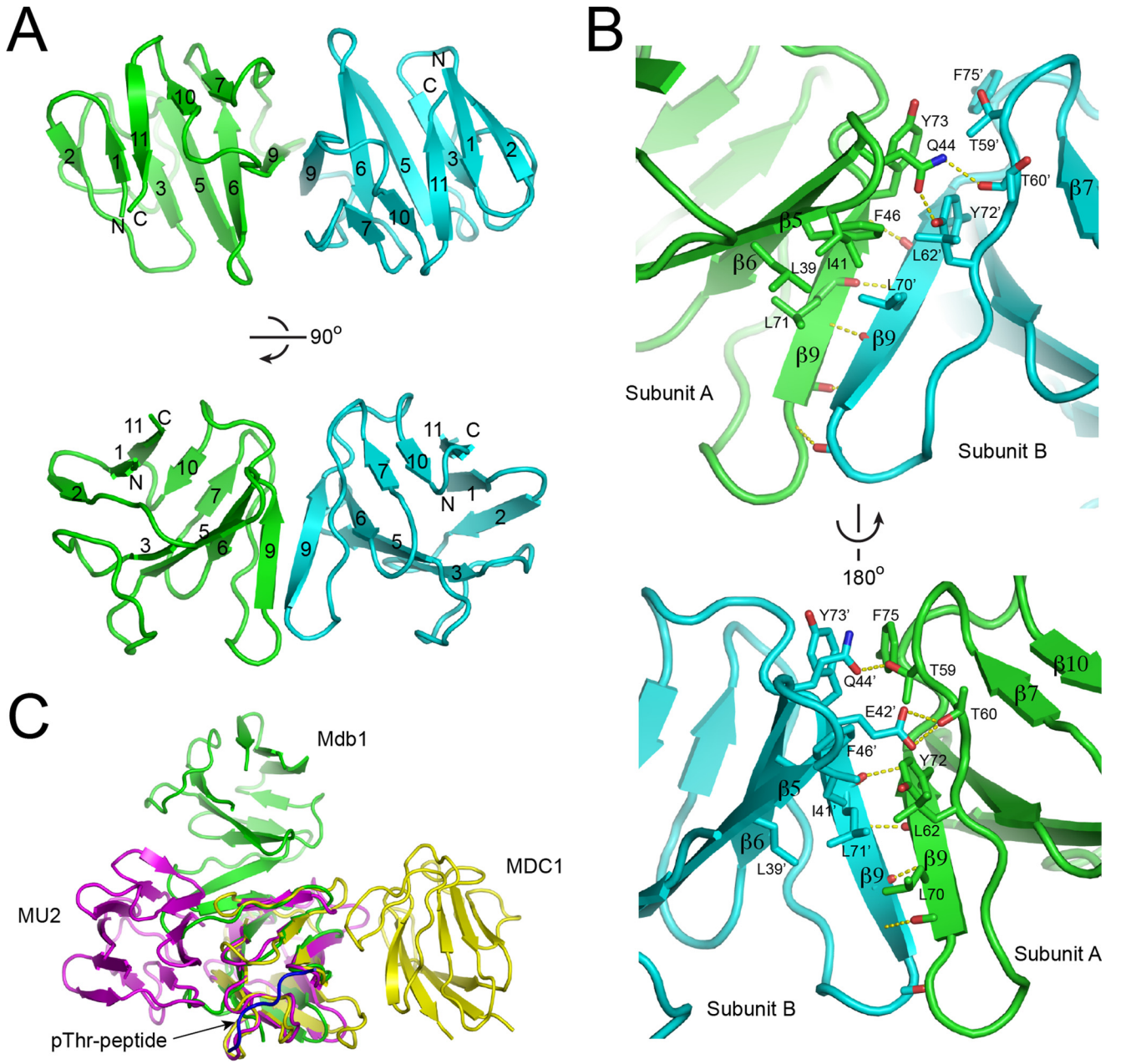

FIGURE 3. **Dimeric structure of Mdb1-FHA.** *A*, ribbon representation of Mdb1-FHA dimer structure shown in two orthogonal views. Subunits A and B are colored *green* and *cyan*, respectively. The β-strands are numbered as in Fig. 2, and the N and C termini are labeled. *B*, the dimer interface viewed from two opposite sides. Residues involved in dimerization are shown as sticks with oxygen colored *red* and nitrogen colored *blue*. Hydrogen bonds are shown as *yellow dashed lines*. *C*, one subunit of the FHA dimers of Mdb1 (*green*), MU2 (*magenta*), and MDC1 (*yellow*) are aligned. The bound Thr(P)-peptide of MDC1 is shown in *blue*.

with a dyad axis, but with a "screw" axis with one residue translation along the β9 strand.

Although the FHA domains of MDC1, MU2, and Mdb1 all form a dimer, their dimerization interfaces are dramatically different (Fig. 3*C*). All three dimerization interfaces are on the lateral surfaces of the β-sandwich, away from the apical surface that binds phosphopeptide in canonical FHA domains. The MDC1 and MU2 interfaces largely correspond to the outer surfaces of the two β-sheets, respectively, whereas the Mdb1 interface is oriented approximately at a right angle from the other two interfaces, situating near an edge of the β-sandwich where the two β-sheets meet.

Analysis with the PISA server shows that the buried solvent-accessible area upon dimerization is 741 Å^2 per subunit, which accounts for 12.6% of the total surface of Mdb1-FHA. Analytical ultracentrifugation sedimentation equilibrium analysis revealed that Mdb1-FHA forms a relative stable dimer with an apparent dissociation constant K_d of 375 nM (Fig. 4, *A* and *B*). As a comparison, the K_d value is 9.2 μM for unphosphorylated MDC1 FHA dimer, 32 nM for MDC1-FHA dimer with a phosphorylated Thr-4, and 0.19 nM for MU2-FHA dimer (10, 12). The different stabilities of these FHA dimers are correlated with the sizes of their dimer interfaces. Mdb1-FHA and MU2-FHA have larger interfaces (741 and 872 Å^2, respectively) and

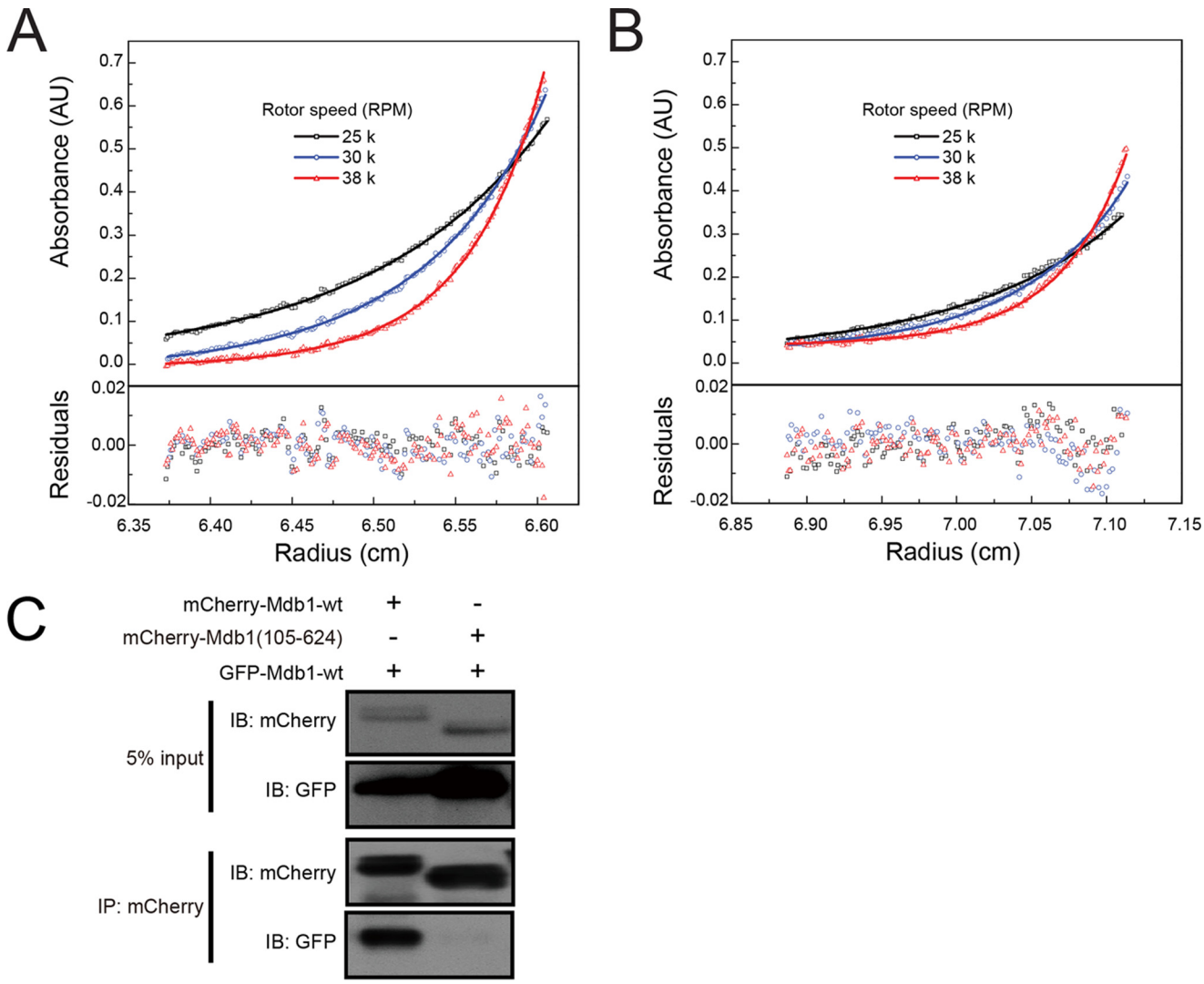

FIGURE 4. **Mdb1-FHA forms a stable dimer *in vitro* and is required for Mdb1 self-interaction *in vivo*.** *A* and *B*, ultracentrifugation sedimentation equilibrium profiles of Mdb1 FHA domain. Proteins in concentrations of 67 μM (*A*) and 34 μM (*B*) were centrifuged at 25,000, 30,000, and 38,000 rpm. The *curves* are the best global fit of the distribution profiles against a self-association model with K_d = 375 nM. Fitting residuals are shown at the *bottom*. *C*, the FHA domain of Mdb1 is required for its self-interaction. mCherry-tagged Mdb1 was immunoprecipitated with RFP-trap agarose beads. The strains used were DY18067 and DY18069. *IB*, immunoblot.

form stable dimer. The MDC1-FHA dimer possesses a smaller interface (490 Å^2) and is unstable in the absence of the trans-interaction with Thr(P)-4.

To verify that Mdb1 dimerization occurs *in vivo*, we co-expressed mCherry-tagged Mdb1 and GFP-tagged Mdb1 together in fission yeast cells and performed a co-immunoprecipitation analysis (Fig. 4*C*). When both tagged proteins were full-length, GFP-tagged Mdb1 was co-immunoprecipitated with mCherry-tagged Mdb1. In contrast, mCherry-tagged Mdb1(105–624), a truncated form of Mdb1 missing the FHA domain, failed to co-immunoprecipitate GFP-tagged full-length Mdb1. Thus, consistent with *in vitro* observations, Mdb1 self-associates in fission yeast in an FHA domain-dependent manner.

FHA-mediated Dimerization Is Important for the Function of Mdb1 in DNA Damage Response—Overexpression of Mdb1 causes genotoxin sensitivity (19). To explore the physiological significance of the FHA-mediated dimerization of Mdb1, we first examined whether the FHA domain is required for the phenotype induced by Mdb1 overexpression (Fig. 5*A*). Compared with the negative control of cells expressing GFP alone from the strong *Pnmt1* promoter, cells expressing full-length Mdb1 tagged with GFP (Mdb1-wt-GFP) exhibited significantly heightened levels of sensitivity to IR, UV, and camptothecin (CPT). In contrast, Mdb1(105–624)-GFP expressed from the same promoter caused a much weaker phenotype, indicating that the FHA domain is important for the overexpression-induced DNA damage sensitivity. Immunoblotting analysis showed that the weaker phenotype induced by Mdb1(105–624)-GFP was not due to a lower expression level (Fig. 5*B*).

To determine whether the defect of the FHA-truncated Mdb1 is due to its inability to dimerize, we employed the strategy of fusing a heterologous dimerization domain (28). If such a domain can rescue the defect, it is likely that dimerization is the main function of the FHA domain. To exclude the remote possibility that the rescuing effect is due to dimerization-unrelated functions of the heterologous sequence, we utilized two completely different types of dimerization modules, GST and a 32-amino acid-long leucine zipper motif (LZ) (28). Both types

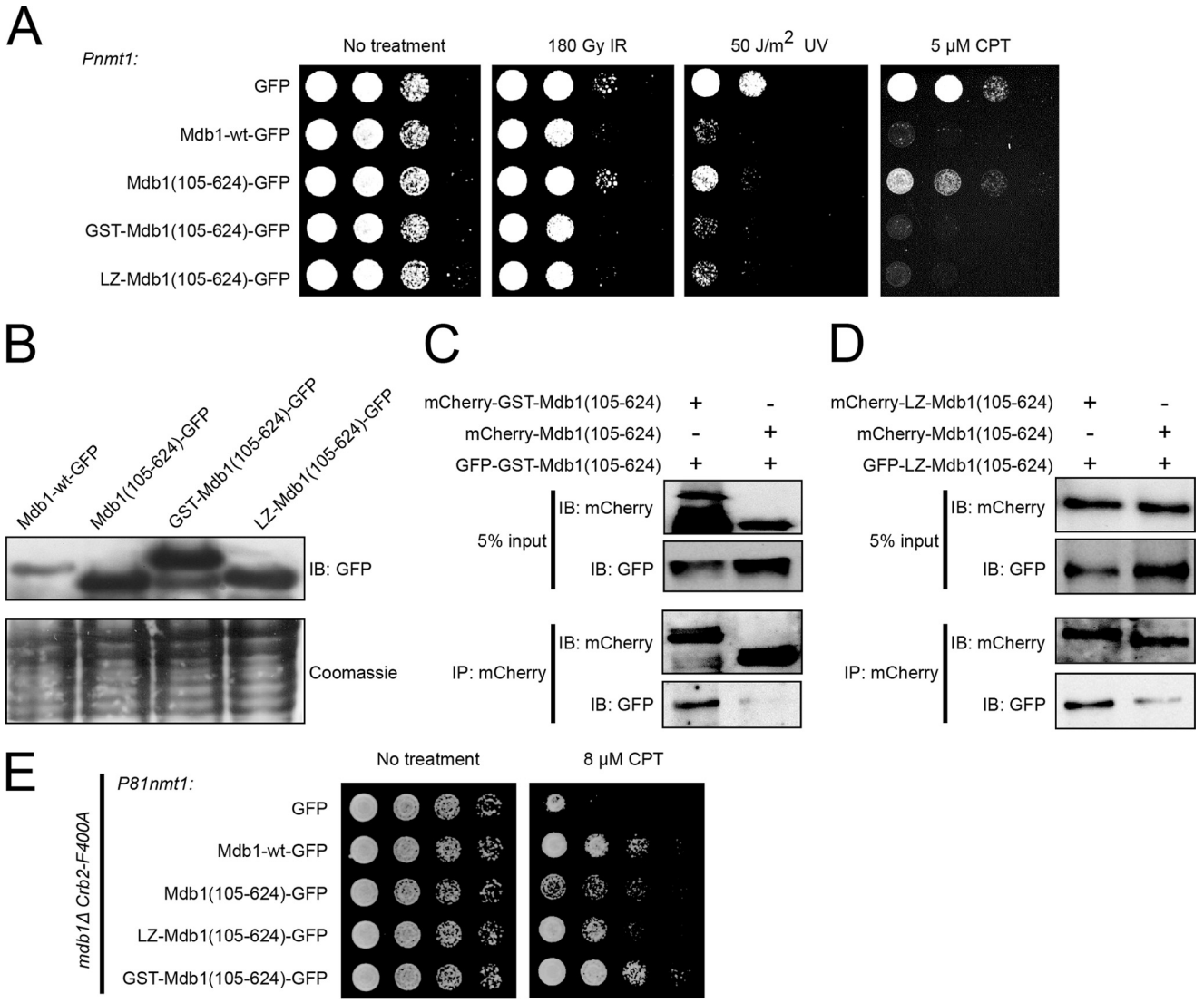

FIGURE 5. **FHA-mediated dimerization is important for the DNA damage functions of Mdb1.** *A*, FHA-mediated dimerization is important for the genotoxin sensitivity induced by Mdb1 overexpression. Cells were pregrown in a thiamine-free medium for 20 h to allow full induction of the *Pnmt1* promoter, and 5-fold serial dilutions were spotted on EMM-based thiamine-free plates. The strains used were DY15615, DY15616, DY17216, DY17218, and DY17220. *B*, the expression levels of different versions of Mdb1 analyzed in *A*. Coomassie staining of PVDF membrane after immunodetection was used to assess protein loading level and blotting efficiency (43). *C*, adding GST tag allowed Mdb1(105–624) to self-interact. The strains used were DY24566 and DY24567. *D*, adding LZ tag allowed Mdb1(105–624) to self-interact. The strains used were DY24570 and DY24571. *E*, FHA-mediated dimerization is required for the ability of Mdb1 to rescue the CPT sensitivity of *mdb1*Δ *crb2-F400A* double mutant. The expression was under the control of the *P81nmt1* promoter. Cells were pregrown in a thiamine-free medium for 20 h before being spotted on CPT-containing thiamine-free plates. The strains used were DY16581, DY17124, DY17126, DY16579, and DY16573. *IB*, immunoblot.

of dimerization domains, when fused to Mdb1(105–624)-GFP, rescued the defect in overexpression-induced DNA damage sensitivity (Fig. 5*A*). Co-immunoprecipitation analysis showed that Mdb1(105–624) fused with either GST or LZ can self-associate, as expected (Fig. 5, *C* and *D*). Thus, dimerization is the main function of Mdb1-FHA in promoting the ability of Mdb1 to cause overexpression-induced genotoxin sensitivity.

Because of the functional redundancy between γH2A interactors in the fission yeast, the phenotypic consequence of Mdb1 loss in DNA damage response can only be observed in strain backgrounds where the function of another γH2A interactor, Crb2, is compromised (19). One of such backgrounds is *crb2-F400A*, a partial loss of function mutation of *crb2*. Deleting *mdb1* in the *crb2-F400A* background dramatically enhances the CPT sensitivity (19). When expressed from the weak promoter *P81nmt1*, Mdb1-GFP rescued the CPT sensitivity of *mdb1*Δ *crb2-F400A* double mutant to a much greater extent than Mdb1(105–624)-GFP (Fig. 5*E*), suggesting that the FHA domain is important for the role of Mdb1 in CPT resistance. Fusing either LZ or GST to Mdb1(105–624)-GFP significantly enhanced its ability to rescue the CPT sensitivity. Thus, dimerization is the main function of Mdb1-FHA in promoting the ability of Mdb1 to confer CPT resistance in the *crb2-F400A* background.

FHA-mediated Dimerization Is Crucial for DNA Damage-induced Mdb1 Focus Formation and the in Vitro Binding of γH2A by Mdb1—The most conserved sequence features of MDC1 family proteins are their C-terminal tBRCT domains, which mediate a direct binding to γH2AX in mammals or γH2A in yeasts. This binding ability allows MDC1 family proteins to accumulate at sites

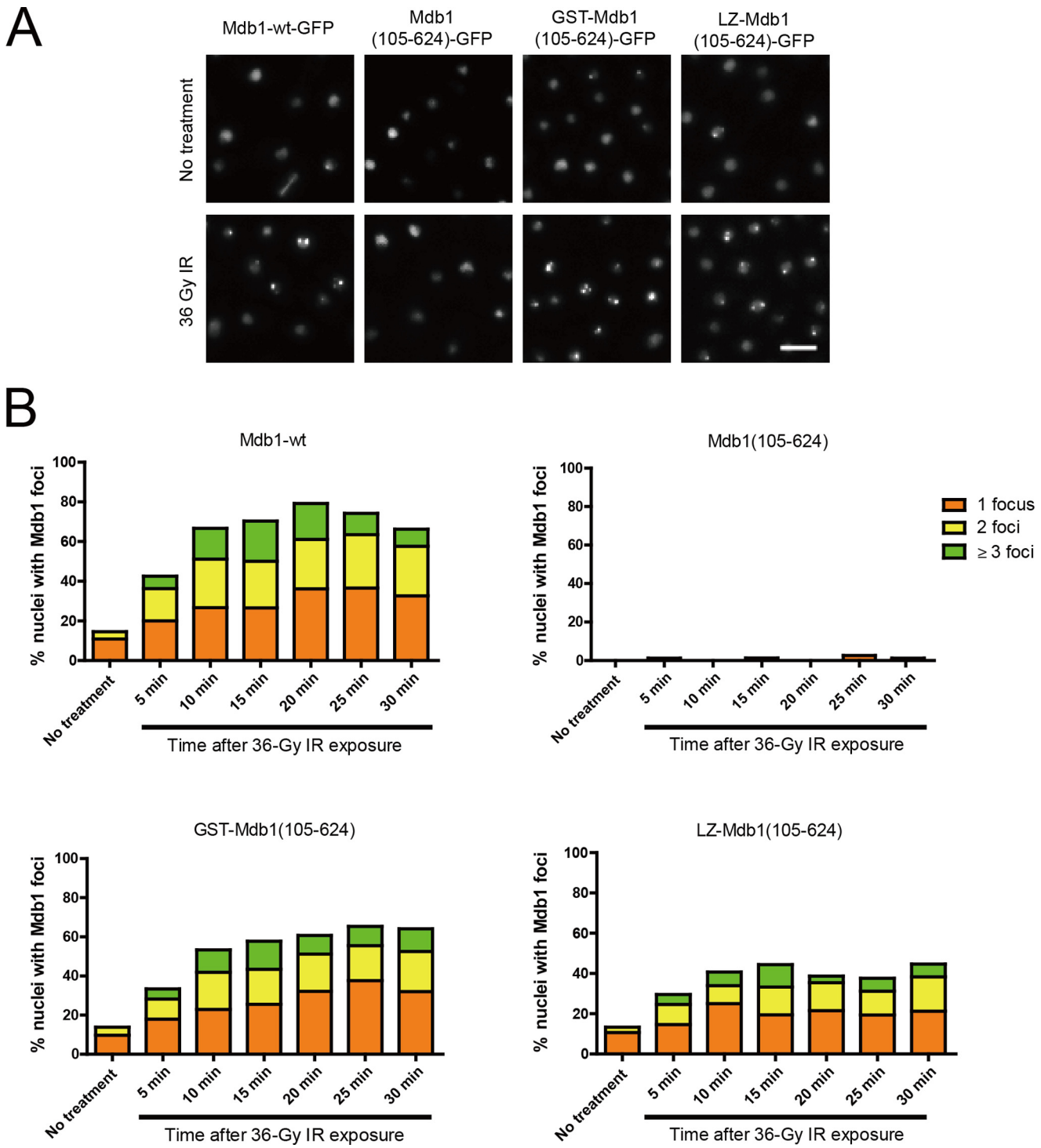

FIGURE 6. **FHA-mediated dimerization is important for the ability of Mdb1 to form nuclear foci.** *A*, focus formation by Mdb1 requires FHA-mediated dimerization. Cells were imaged before and 30 min after exposure to 36 Gy of IR. The strains used were DY15603, DY15638, DY16309, and DY16307. *Bar*, 5 μm. *B*, a time course analysis of IR-induced Mdb1 focus formation. Approximately 200 nuclei were examined for each sample.

of DNA damage and form nuclear foci. It has been shown previously that Mdb1 forms γH2A- and tBRCT domain-dependent nuclear foci at DNA damage sites (19). To probe the role of Mdb1-FHA in the DNA damage-induced relocalization of Mdb1, we used live cell imaging to examine the nuclear focus formation by Mdb1 (Fig. 6, *A* and *B*). Wild-type Mdb1 formed nuclear foci in a small fraction of untreated cells, presumably because of spontaneous DNA damage. IR treatment resulted in a substantially higher level of Mdb1 foci. Truncating the FHA domain completely abolished both spontaneous and IR-induced Mdb1 foci. Fusing either GST or LZ to the truncated Mdb1 rescued the focus formation defect. These results demonstrated that FHA-mediated dimerization is essential for the ability of Mdb1 to concentrate at DNA damage sites.

The nuclear foci data raised the possibility that dimerization is important for the γH2A binding ability of Mdb1. To test this

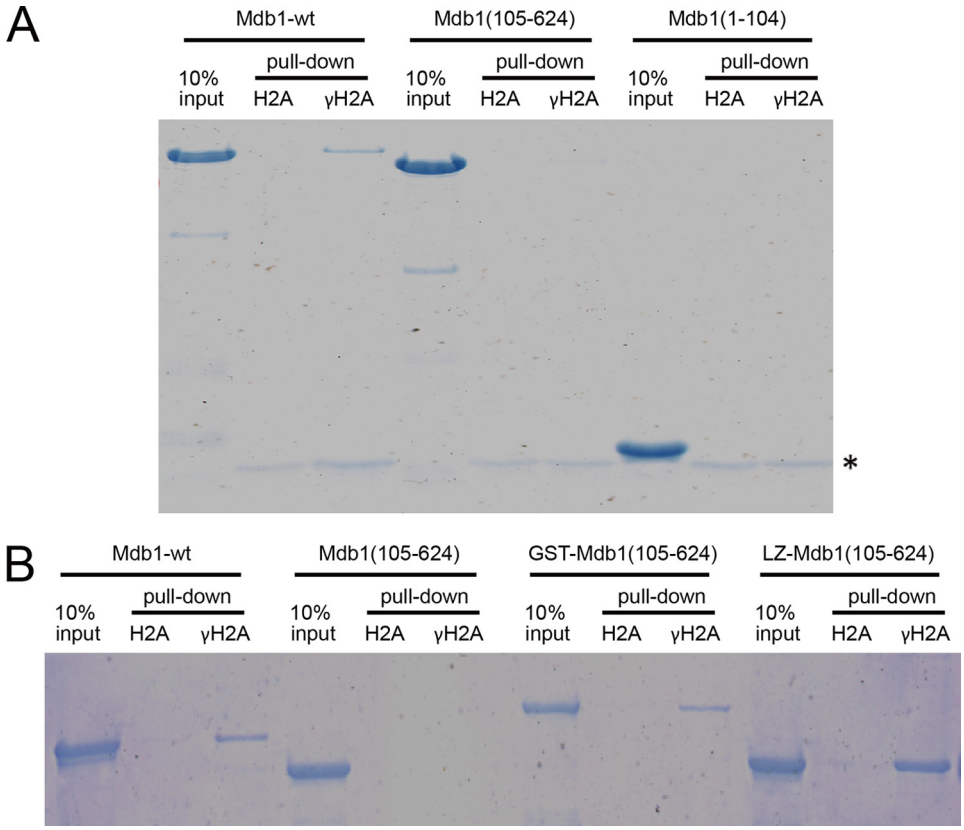

FIGURE 7. **FHA-mediated dimerization is important for the ability of Mdb1 to interact with γH2A.** *A*, the FHA domain is necessary but not sufficient for Mdb1 to bind γH2A. Recombinant Mdb1 proteins were expressed in bacteria and purified using the His_6 tag. Biotinylated peptides that correspond to the C terminus of H2A.1, either unmodified (H2A) or phosphorylated on Ser-129 (γH2A), were incubated with the recombinant Mdb1 proteins. Peptides and associated proteins were pulled down by streptavidin Dynabeads and eluted by boiling in SDS-PAGE loading buffer. The eluates and 10% inputs were analyzed by SDS-PAGE followed by Coomassie staining. The *asterisk* indicates a background band released from the Dynabeads. *B*, adding a dimerization domain rescued the ability of Mdb1(105–624) to interact with γH2A. The experiment was performed as in *A*.

idea, we performed *in vitro* peptide pulldown assay (Fig. 7). Recombinant full-length Mdb1 could be pulled down by a γH2A peptide. Neither Mdb1(105–624) nor Mdb1(1–104) showed a detectable interaction with the γH2A peptide (Fig. 7*A*). Both GST fusion and LZ fusion restored the ability of Mdb1(105–624) to bind γH2A (Fig. 7*B*). These results led us to conclude that FHA-mediated dimerization promotes the ability of Mdb1 to bind γH2A.

Mdb1 Focus Formation Requires Both Subunits in a Dimer to Be Able to Bind γH2A—The importance of dimerization for Mdb1 to form γH2A-dependent nuclear foci *in vivo* and bind a γH2A peptide *in vitro* suggests that the tBRCT domains in both subunits of an Mdb1 dimer need to interact with γH2A. To test this idea, we adopted an approach of constructing an artificial heterodimer (30). We fused a monomeric GFP-binding protein (GBP) to Mdb1(105–624), so that it can form a heterodimer with GFP-tagged Mdb1(105–624). Co-expression of Mdb1(105–624)-GBP rescued the ability of Mdb1(105–624)-GFP to form nuclear foci (Fig. 8), indicating that heterodimerization mediated by the GBP-GFP interaction is sufficient to substitute for FHA-mediated homodimerization. When we introduced K434M, a tBRCT domain mutation that disrupts γH2A binding (19), to either one or both of the subunits in the heterodimer, focus formation by Mdb1(105–624)-GFP was abolished (Fig. 8). Thus, a functional Mdb1 dimer requires both tBRCT domains to be capable of binding γH2A.

FHA-mediated Dimerization Is Important for the Spindle Function of Mdb1—Mdb1 localizes to the spindle midzone during mitosis in a tBRCT domain-dependent but γH2A-independent manner, presumably because of a phosphorylation-dependent interaction with a yet to be identified spindle component (19). To analyze whether the FHA domain is important for the midzone localization, we imaged mitotic cells (Fig. 9). Truncating the FHA domain abolished the midzone localization in anaphase cells, but this defect could be rescued by fusing with either GST or LZ. Thus, the FHA domain is required for midzone localization, and its main role in this process is mediating dimerization.

Likely related to the spindle midzone localization of Mdb1, it was shown that loss of Mdb1 causes a resistance to the microtubule-destabilizing drug thiabendazole (TBZ) (19). This phenotype could be reversed by the expression of wild-type but not FHA-truncated Mdb1 (Fig. 10). Fusing either GST or LZ to the truncated Mdb1 allowed it to reverse the TBZ-resistant phenotype of *mdb1*Δ (Fig. 10). Thus, FHA-mediated dimerization is important for the role of Mdb1 in conferring a normal level of TBZ resistance.

Discussion

Dimerization Is the Main Function of Mdb1-FHA—In this study, we present multiple lines of evidence including crystal structure, gel filtration, analytical ultracentrifugation, and co-immunoprecipitation to show that Mdb1-FHA forms a homodimer. Furthermore, we show that loss of FHA domain

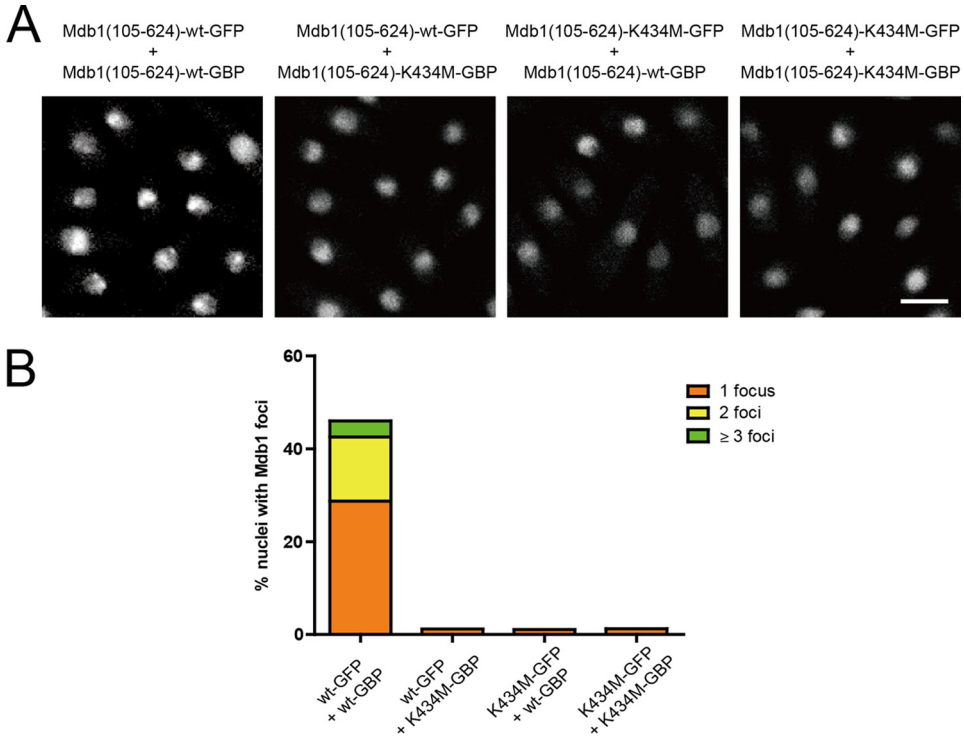

FIGURE 8. **Mdb1 focus formation requires both subunits in a dimer to possess the γH2A-binding ability.** *A*, co-expression of Mdb1(105–624)-GBP rescued the ability of Mdb1(105–624)-GFP to form nuclear foci, and this rescue was abolished when the K434M mutation was introduced into one or both proteins. Cells were imaged 30 min after exposure to 36 Gy of IR. The strains used were DY23263, DY24110, DY24112, and DY24114. *Bar*, 5 μm. *B*, quantitation of the results shown in *A*. Approximately 200 nuclei were examined for each sample.

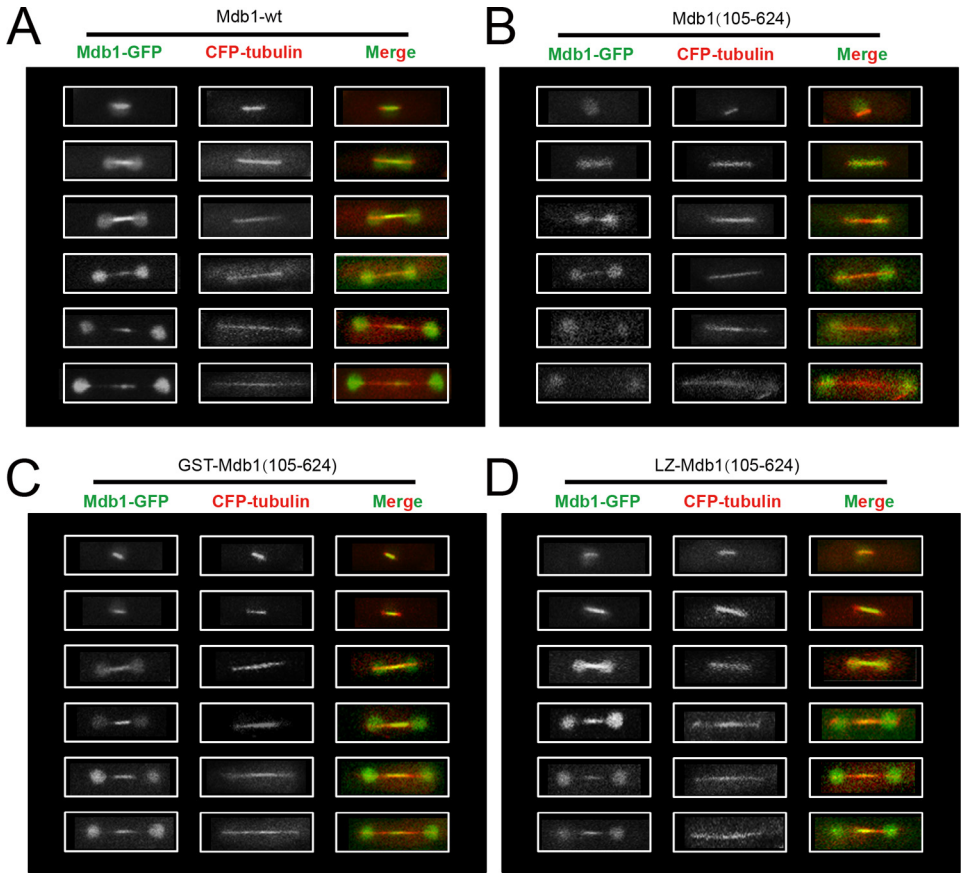

FIGURE 9. **The midzone accumulation of Mdb1 requires FHA-mediated dimerization.** The strains used were DY15627, DY16639, DY16643, and DY16645. *A*, Mdb1-wt. *B*, Mdb1(105–624). *C*, GST-Mdb1(105–624). *D*, LZ-Mdb1(105–624).

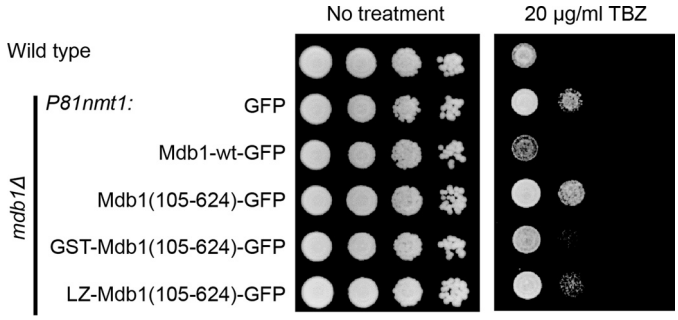

FIGURE 10. **FHA-mediated dimerization is important for the ability of Mdb1 to reverse the TBZ-resistant phenotype of *mdb1*Δ.** Cells were pregrown in a thiamine-free medium for 20 h before being spotted on TBZ-containing thiamine-free plates. The strains used were LD327, DY15630, DY15603, DY15638, DY16309, and DY16307.

severely compromises the functions of Mdb1 in DNA damage response and spindle regulation. The defect of FHA-truncated Mdb1 in DNA damage response can be attributed to its inability to bind γH2A. This is not due to a direct role of Mdb1-FHA in γH2A binding because, first, Mdb1-FHA lacks phospho-binding residues; second, γH2A-binding requires the phospho-binding residues in the tBRCT domain (19); third, recombinant Mdb1-FHA failed to bind γH2A *in vitro*; and finally, fusing a heterologous dimerization domain rescues the γH2A binding defect caused by FHA truncation. Together, our results demonstrate that the main role of Mdb1-FHA is mediating homodimerization, which is important for the physiological functions of Mdb1.

Why Homodimerization Is Important for Mdb1—Accumulating evidence suggests that dimerization/oligomerization is a common property of DNA damage response proteins. The best known examples in this regard are the tandem Tudor (tTudor) domain- and tBRCT domain-containing proteins in the Rad9/Crb2/53BP1 family (15, 28, 31–36). Approaches such as the fusion strategy used in this study have unequivocally demonstrated the functional importance of dimerization/oligomerization for Rad9, Crb2, and 53BP1. However, the reasons why dimerization/oligomerization is important remain largely unclear. In this study, we showed by a peptide pulldown assay that a normal γH2A-binding ability of Mdb1 requires its dimerization. This is likely due to the presence of a large number of γH2A peptides on the beads so that both subunits of the Mdb1 dimer can engage in tBRCT-γH2A interactions simultaneously, resulting in a much higher avidity than monomeric interactions. We would like to argue that the interactions with bead-bound γH2A peptides are not unlike the *in vivo* binding to γH2A molecules, which can be present at two copies per nucleosome. The long linker between FHA and tBRCT domains may also allow simultaneous binding to two γH2A molecules not in the same, but in adjacent nucleosomes. Thus, the same avidity effect may explain why dimeric but not monomeric Mdb1 can form γH2A-dependent nuclear foci *in vivo*. This model is supported by the GBP-GFP heterodimerization results. However, we cannot rule out the possibility that dimerization may enhance γH2A binding through other mechanisms, such as relieving inhibition imposed by the linker region or the formation of a new γH2A binding interface.

Evolutionary Conservation and Plasticity of FHA-mediated Dimerization of MDC1 Family Proteins—FHA domains are notable for their lack of sequence conservation. Only five of ~100 residues are strictly conserved in the great majority of FHA domains (37). These five residues (Gly-57, Arg-58, Ser-72, His-75, and Asn-96 in MDC1) are either directly or indirectly involved in phosphopeptide binding (38). Remarkably, none of these five residues are conserved in Mdb1 (Fig. 2*C*), explaining why domain-searching tools fail to recognize the N-terminal sequence of Mdb1 as an FHA domain. Despite the extreme sequence divergence, the conservation of the three-dimensional fold indicates that in addition to the tBRCT domain, Mdb1 is also related to MDC1 in the FHA domain, thus definitively establishing that Mdb1 is an ortholog of MDC1.

The structures of dozens of different FHA domains have been determined (39, 37). Among the previously published FHA structures, in addition to those of MDC1 and MU2, only two FHA domains, the ones from CHFR and kanadaptin, have been reported to form homodimers (40, 41). However, both CHFR-FHA and kanadaptin-FHA exist as monomers in solution, and thus the dimers observed in the crystals may not be physiologically relevant. The rarity of FHA domains that can form stable homodimers suggests that homodimerization is not an easily evolved ability of FHA domains and argues against the idea that MDC1, MU2, and Mdb1 have independently acquired this ability after diverging from a monomeric ancestor protein. We favor the scenario in which the FHA domains of MDC1-like proteins in the common ancestors of animals and fungi possessed both the ability to homodimerize and the ability to bind phosphopeptides, and the latter ability was lost in the lineages leading to *Drosophila* and fission yeasts.

If dimerization is indeed an ancient and important function of the FHA domains of the MDC1 family proteins, the divergence of the dimer interfaces in MDC1, MU2, and Mdb1 suggests a surprising plasticity of the FHA domains to fulfill the same evolutionarily constrained function through variable structural means. The Mdb1 dimer structure we report here adds a distinctly new example to the increasingly diverse protein interaction modes of FHA domains (42).

Author Contributions—S. L. performed the biophysical and structural analyses of Mdb1-FHA. X. X. and Y. W. performed the experiments using fission yeast. L.-L. D. and K. Y. conceived and coordinated the study. L.-L. D., K. Y., S. L., and Y. W. wrote the paper. All authors reviewed the results and approved the final version of the manuscript.

Acknowledgments—We thank the staff at the Beijing Synchrotron Radiation Facility Beamline 3W1A for assistance in diffraction data collection, Xiaoxia Yu (Institute of Biophysics, Chinese Academy of Sciences) for ultracentrifugation experiments. We thank Hong-Chang Zhao for contributions at an early stage of the project and Li-Xue Diao for plasmid constructions.

References

1. Reinhardt, H. C., and Yaffe, M. B. (2013) Phospho-Ser/Thr-binding domains: navigating the cell cycle and DNA damage response. *Nat. Rev. Mol. Cell Biol.* **14,** 563–580
2. Mermershtain, I., and Glover, J. N. (2013) Structural mechanisms underlying signaling in the cellular response to DNA double strand breaks.

Mutat. Res. **750,** 15–22
3. Rogakou, E. P., Pilch, D. R., Orr, A. H., Ivanova, V. S., and Bonner, W. M. (1998) DNA double-stranded breaks induce histone H2AX phosphorylation on serine 139. *J. Biol. Chem.* **273,** 5858–5868
4. Scully, R., and Xie, A. (2013) Double strand break repair functions of histone H2AX. *Mutat. Res.* **750,** 5–14
5. Stucki, M., Clapperton, J. A., Mohammad, D., Yaffe, M. B., Smerdon, S. J., and Jackson, S. P. (2005) MDC1 directly binds phosphorylated histone H2AX to regulate cellular responses to DNA double-strand breaks. *Cell.* **123,** 1213–1226
6. Lou, Z., Minter-Dykhouse, K., Franco, S., Gostissa, M., Rivera, M. A., Celeste, A., Manis, J. P., van Deursen, J., Nussenzweig, A., Paull, T. T., Alt, F. W., and Chen, J. (2006) MDC1 maintains genomic stability by participating in the amplification of ATM-dependent DNA damage signals. *Mol. Cell* **21,** 187–200
7. Lee, M. S., Edwards, R. A., Thede, G. L., and Glover, J. N. (2005) Structure of the BRCT repeat domain of MDC1 and its specificity for the free COOH-terminal end of the gamma-H2AX histone tail. *J. Biol. Chem.* **280,** 32053–32056
8. Luo, K., Yuan, J., and Lou, Z. (2011) Oligomerization of MDC1 protein is important for proper DNA damage response. *J. Biol. Chem.* **286,** 28192–28199
9. Wu, H.-H., Wu, P.-Y., Huang, K.-F., Kao, Y.-Y., and Tsai, M.-D. (2012) Structural delineation of MDC1-FHA domain binding with CHK2-pThr68. *Biochemistry* **51,** 575–577
10. Liu, J., Luo, S., Zhao, H., Liao, J., Li, J., Yang, C., Xu, B., Stern, D. F., Xu, X., and Ye, K. (2012) Structural mechanism of the phosphorylation-dependent dimerization of the MDC1 forkhead-associated domain. *Nucleic Acids Res.* **40,** 3898–3912
11. Jungmichel, S., Clapperton, J. A., Lloyd, J., Hari, F. J., Spycher, C., Pavic, L., Li, J., Haire, L. F., Bonalli, M., Larsen, D. H., Lukas, C., Lukas, J., MacMillan, D., Nielsen, M. L., Stucki, M., and Smerdon, S. J. (2012) The molecular basis of ATM-dependent dimerization of the Mdc1 DNA damage checkpoint mediator. *Nucleic Acids Res.* **40,** 3913–3928
12. Luo, S., and Ye, K. (2012) Dimerization, but not phosphothreonine binding, is conserved between the forkhead-associated domains of *Drosophila* MU2 and human MDC1. *FEBS Lett.* **586,** 344–349
13. Nakamura, T. M., Du, L.-L., Redon, C., and Russell, P. (2004) Histone H2A phosphorylation controls Crb2 recruitment at DNA breaks, maintains checkpoint arrest, and influences DNA repair in fission yeast. *Mol. Cell. Biol.* **24,** 6215–6230
14. Du, L.-L., Nakamura, T. M., and Russell, P. (2006) Histone modification-dependent and -independent pathways for recruitment of checkpoint protein Crb2 to double-strand breaks. *Genes Dev.* **20,** 1583–1596
15. Kilkenny, M. L., Doré, A. S., Roe, S. M., Nestoras, K., Ho, J. C., Watts, F. Z., and Pearl, L. H. (2008) Structural and functional analysis of the Crb2-BRCT2 domain reveals distinct roles in checkpoint signaling and DNA damage repair. *Genes Dev.* **22,** 2034–2047
16. Sofueva, S., Du, L.-L., Limbo, O., Williams, J. S., and Russell, P. (2010) BRCT domain interactions with phospho-histone H2A target Crb2 to chromatin at double-strand breaks and maintain the DNA damage checkpoint. *Mol. Cell. Biol.* **30,** 4732–4743
17. Rozenzhak, S., Mejía-Ramírez, E., Williams, J. S., Schaffer, L., Hammond, J. A., Head, S. R., and Russell, P. (2010) Rad3 decorates critical chromosomal domains with gammaH2A to protect genome integrity during S-Phase in fission yeast. *PLoS Genet.* **6,** e1001032
18. Williams, J. S., Williams, R. S., Dovey, C. L., Guenther, G., Tainer, J. A., and Russell, P. (2010) γH2A binds Brc1 to maintain genome integrity during S-phase. *EMBO J.* **29,** 1136–1148
19. Wei, Y., Wang, H.-T., Zhai, Y., Russell, P., and Du, L.-L. (2014) Mdb1, a fission yeast homolog of human MDC1, modulates DNA damage response and mitotic spindle function. *PLoS One* **9,** e97028
20. Otwinowski, Z., and Minor, W. (1997) Processing of x-ray diffraction data collected in oscillation mode. *Methods Enzymol.* **276,** 307–326
21. Vonrhein, C., Blanc, E., Roversi, P., and Bricogne, G. (2007) Automated structure solution with autoSHARP. *Methods Mol. Biol.* **364,** 215–230
22. Emsley, P., and Cowtan, K. (2004) Coot: model-building tools for molecular graphics. *Acta Crystallogr. D Biol. Crystallogr.* **60,** 2126–2132
23. Murshudov, G. N., Vagin, A. A., Lebedev, A., Wilson, K. S., and Dodson, E. J. (1999) Efficient anisotropic refinement of macromolecular structures using FFT. *Acta Crystallogr. D Biol. Crystallogr.* **55,** 247–255
24. Adams, P. D., Afonine, P. V., Bunkóczi, G., Chen, V. B., Davis, I. W., Echols, N., Headd, J. J., Hung, L.-W., Kapral, G. J., Grosse-Kunstleve, R. W., McCoy, A. J., Moriarty, N. W., Oeffner, R., Read, R. J., Richardson, D. C., Richardson, J. S., Terwilliger, T. C., and Zwart, P. H. (2010) PHENIX: a comprehensive Python-based system for macromolecular structure solution. *Acta Crystallogr. D Biol. Crystallogr.* **66,** 213–221
25. DeLano, W. L. (2002) *The PyMOL User's Manual*, DeLano Scientific, San Carlos, CA
26. Forsburg, S. L., and Rhind, N. (2006) Basic methods for fission yeast. *Yeast* **23,** 173–183
27. Matsuyama, A., Shirai, A., Yashiroda, Y., Kamata, A., Horinouchi, S., and Yoshida, M. (2004) pDUAL, a multipurpose, multicopy vector capable of chromosomal integration in fission yeast. *Yeast* **21,** 1289–1305
28. Du, L.-L., Moser, B. A., and Russell, P. (2004) Homo-oligomerization is the essential function of the tandem BRCT domains in the checkpoint protein Crb2. *J. Biol. Chem.* **279,** 38409–38414
29. Holm, L., and Rosenström, P. (2010) Dali server: conservation mapping in 3D. *Nucleic Acids Res.* **38,** W545–W549
30. Qu, M., Rappas, M., Wardlaw, C. P., Garcia, V., Ren, J.-Y., Day, M., Carr, A. M., Oliver, A. W., Du, L.-L., and Pearl, L. H. (2013) Phosphorylation-dependent assembly and coordination of the DNA damage checkpoint apparatus by Rad4(TopBP1). *Mol. Cell.* **51,** 723–736
31. Soulier, J., and Lowndes, N. F. (1999) The BRCT domain of the S. cerevisiae checkpoint protein Rad9 mediates a Rad9-Rad9 interaction after DNA damage. *Curr. Biol.* **9,** 551–554
32. Usui, T., Foster, S. S., and Petrini, J. H. (2009) Maintenance of the DNA-damage checkpoint requires DNA-damage-induced mediator protein oligomerization. *Mol. Cell.* **33,** 147–159
33. Granata, M., Lazzaro, F., Novarina, D., Panigada, D., Puddu, F., Abreu, C. M., Kumar, R., Grenon, M., Lowndes, N. F., Plevani, P., and Muzi-Falconi, M. (2010) Dynamics of Rad9 chromatin binding and checkpoint function are mediated by its dimerization and are cell cycle-regulated by CDK1 activity. *PLoS Genet.* **6,** e1001047
34. Adams, M. M., Wang, B., Xia, Z., Morales, J. C., Lu, X., Donehower, L. A., Bochar, D. A., Elledge, S. J., and Carpenter, P. B. (2005) 53BP1 oligomerization is independent of its methylation by PRMT1. *Cell Cycle* **4,** 1854–1861
35. Ward, I., Kim, J.-E., Minn, K., Chini, C. C., Mer, G., and Chen, J. (2006) The tandem BRCT domain of 53BP1 is not required for its repair function. *J. Biol. Chem.* **281,** 38472–38477
36. Zgheib, O., Pataky, K., Brugger, J., and Halazonetis, T. D. (2009) An oligomerized 53BP1 tudor domain suffices for recognition of DNA double-strand breaks. *Mol. Cell. Biol.* **29,** 1050–1058
37. Huang, Y. M., and Chang, C.-E. A. (2014) Achieving peptide binding specificity and promiscuity by loops: case of the forkhead-associated domain. *PLoS One* **9,** e98291
38. Durocher, D., Taylor, I. A., Sarbassova, D., Haire, L. F., Westcott, S. L., Jackson, S. P., Smerdon, S. J., and Yaffe, M. B. (2000) The molecular basis of FHA domain:phosphopeptide binding specificity and implications for phospho-dependent signaling mechanisms. *Mol. Cell* **6,** 1169–1182
39. Mahajan, A., Yuan, C., Lee, H., Chen, E. S.-W., Wu, P.-Y., and Tsai, M.-D. (2008) Structure and function of the phosphothreonine-specific FHA domain. *Sci. Signal.* **1,** re12
40. Stavridi, E. S., Huyen, Y., Loreto, I. R., Scolnick, D. M., Halazonetis, T. D., Pavletich, N. P., and Jeffrey, P. D. (2002) Crystal structure of the FHA domain of the Chfr mitotic checkpoint protein and its complex with tungstate. *Structure* **10,** 891–899
41. Xu, Q., Deller, M. C., Nielsen, T. K., Grant, J. C., Lesley, S. A., Elsliger, M.-A., Deacon, A. M., and Wilson, I. A. (2014) Structural insights into the recognition of phosphopeptide by the FHA domain of kanadaptin. *PLoS One* **9,** e107309
42. Matthews, L. A., and Guarne, A. (2013) Extending the interaction repertoire of FHA and BRCT domains. In *The Mechanisms of DNA Replication* (Stuart, D., ed) InTech, Rijeka, Croatia
43. Welinder, C., and Ekblad, L. (2011) Coomassie staining as loading control in Western blot analysis. *J. Proteome Res.* **10,** 1416–1419